

A Survey of the HCN $J=1-0$ Hyperfine Lines towards Class 0 and I Sources

Y.-S. Park^{1,2}, Jongsoo Kim¹, and Y. C. Minh¹

Received _____; accepted _____

¹Korea Astronomy Observatory, San 36-1, Hwaam-dong, Yusung, Taejon, 305-348, Korea

²Institute of Astronomy and Astrophysics, Academia Sinica, P.O. Box 1-87, Nankang, Taipei, Taiwan 115, R.O.C., e-mail: yspark@asiaa.sinica.edu.tw

ABSTRACT

The HCN 1–0 hyperfine lines have been observed toward 24 young stellar objects (YSOs) of class 0 and I. The hyperfine lines are well separated in most cases and show such rich structures as asymmetric double peaks and strong wings. We examined how their line shapes and velocity shifts vary along with their relative optical depths and compared them with those of CS 2–1, H₂CO 2₁₂–1₁₁, and HCO⁺ 4–3 & 3–2 transitions previously observed by Mardones et al. (1997) and Gregersen et al. (1997).

It is found that all these molecular species do not always exhibit the same sense of line asymmetry and the correlation of velocity shift is better between HCN and CS than between HCN and H₂CO. The most opaque transition of HCN $F=2-1$ has about the same velocity shift as that of CS despite of the larger beam size of this study, which suggests that HCN $F=2-1$ line may be more sensitive to the internal motion of YSOs than CS line. Systematic changes of the velocity shift are noted for many sources, as one goes from $F=0-1$ to $2-1$. The monotonic decrease of velocity (blue shift) is apparently more frequent.

A detailed model of radiative transfer allowing line overlap of HCN is employed to L483 which shows convincing signatures of infall on a scale of ~ 0.1 pc. It appears that the observed line is not compatible with the standard Shu (1977) model, but is fitted with augmentations of density and infall velocity, by factors of 6 and 0.5, respectively, and with an inclusion of a diffuse, static, turbulent, and geometrically thick envelope.

The distribution of hyperfine line intensity ratios for these YSOs does not accord with the LTE condition and is essentially the same as ones previously noted in cold dark clouds or small translucent cores. Though this anomaly may be explained in terms of radiative transfer effect in the cores which are either

static or under systematic motion, some of them seem to invoke an existence of scattering envelope. It is confirmed that HCN is detected more selectively in class 0 and I sources than in starless cores or class II objects, which implies that the core embedding YSO(s) form a dense ($\sim 10^6 \text{cm}^{-3}$) envelope with a significant HCN abundance in a narrow time span of their evolution (Afonso et al. 1998).

Subject headings:

1. Introduction

Since the pioneering works of Zhou and his colleagues (Zhou et al. 1993; Zhou et al. 1994; Zhou 1995), observational signatures of infall motion in the early phase of star formation have been discovered towards many young stellar objects (YSOs). They are mainly based on the spectral features that an opaque molecular line has a self-absorption with the blue peak stronger than the red one (hereafter the blue asymmetry), while an optically thin line of single peak is located between the two peaks of the opaque one. In an attempt to search for infalling YSOs, surveys of class 0 and I sources have been undertaken using the transitions of, e.g., CS, H₂CO, and HCO⁺. However, only a few sources like B335 and IRAS 16293–2422 seem to provide compelling evidence of collapse motion (Zhou et al. 1993; Zhou 1995; Narayanan et al. 1998). Line profiles of some sources exhibit different asymmetry from one molecular species to another as well as from transition to transition in a molecule (Mardones et al. 1997; Lehtinen 1997; Gregersen et al. 1997). It is likely that the infall motion is not so simple or monotonic as one expects. Not only outflow motion but also aspherical geometry make the problem more complex. Thus, previous studies have always come to a conservative conclusion that class 0 objects seem to undergo infall phase in a statistical sense only and it is unclear for class I objects (Mardones et al. 1997; Gregersen et al. 1997).

In order to have a comprehensive view on the internal motion of YSOs, one needs to make observations with various molecules and transitions using both single dish and interferometer. As a complement to the previous single dish observations by Mardones et al. (1997) and by Gregersen et al. (1997), we have carried out an HCN $J=1-0$ survey of class 0 and I YSOs. We can probe denser regions with HCN $J=1-0$ lines than with CS $J=2-1$ one, the most popular density tracer. The $J=1-0$ transition of HCN has three hyperfine lines ($F=1-0$, $1-1$, and $2-1$) whose optical depths are scaled to 1 : 3 : 5 in the

LTE condition. The hyperfine lines enable us to investigate how the line shape changes with their optical depths. Moreover, molecular abundance and spatial resolutions are the same for the three hyperfine components. This is an advantage over using other combinations of molecules or transitions with different beam sizes or abundances. Recently, it is known that the HCN emission peak of each Bok globule is coincident with the position of embedded source within 6'' and the detection rate of HCN lines is higher in class I and probably class 0 sources than in starless cores and class II sources (Afonso et al. 1998). Thus HCN may be a good tracer of class 0 and I objects.

The main goal of this study is to provide another set of line profiles of YSOs. Based on the data set, we investigate the tendency of line asymmetry among three hyperfine components, compare the asymmetry with that of other molecular lines, and probe the internal structure and kinematics of the cores. Probing with various molecular species may also be helpful in investigating molecular chemistry in the protostellar cores (Rawlings 1996).

After presenting observation and data reduction procedure (section 2), we describes observational results in section 3. A simple radiative transfer model of L483 is detailed in section 4. Discussions on the relevant molecular chemistry and hyperfine line ratios of HCN are given in section 5. Finally, we summarize results in section 6.

2. Observations

The sources listed in Table 1 have been selected based on the data set in Mardones et al. (1997) and Gregersen et al. (1997). We detected HCN hyperfine lines toward 22 of 24 with an rms level of a few tens of mK.

Observations were carried out with a radome-enclosed 14 meter telescope in Taeduk

Radio Astronomy Observatory, Korea, during April and May 1997. We used an SIS receiver and an autocorrelation spectrometer with 20 KHz (0.068 km s^{-1} at HCN $F=2-1$ frequency) resolution. System temperatures were typically $400 - 600 \text{ K}$ (SSB) and pointing was good to an accuracy of $10''$ in both directions of azimuth and elevation. The spectra were Hanning-smoothed, calibrated by a standard chopper wheel method, and presented in an antenna temperature (T_A^*) scale.

The rest frequency of $F=2-1$ transition is 88.631847 GHz, and the separations of $F=1-1$ and $F=0-1$ lines with respect to $F=2-1$ are 4.84 and -7.07 km s^{-1} , respectively (Lovas 1992). Measured FWHM beam size and beam efficiency are $61''$ and 40%, respectively, at this frequency. We used frequency switching mode with $\Delta f = 6 \text{ MHz}$ and obtained the spectra with the S/N ratios better than 15.

3. Results

3.1. Line profiles

Observed line profiles are presented in Fig. 1 (a-d), where we see spectral features like self-absorption, asymmetry, and broad wings. The hyperfine lines are well separated except for a few cases. Line asymmetries of many sources seem to grow as the optical depth increases. All three hyperfine lines appear to be optically thin for L146, Serp SMM3, L673A, and L1152, whereas they all are optically thick for NGC1333-4A, L483, and B335. The line wings of many sources are generally weaker than those in other studies (Mardones et al. 1997; Gregersen et al. 1997), which may result from a larger telescope beam of this study.

3.2. Individual sources

We outline the characteristics of HCN line profiles of the sources and, when available, compare them with those of CS 2–1, H₂CO 2₁₂–1₁₁, and N₂H⁺ 1–0 in Mardones et al. (1997) and with HCO⁺ 4–3 and 3–2 in Gregersen et al. (1997). Mainly sources with dissimilarities in line shapes among molecular species are discussed. It should be noted that the two surveys are made with FWHM beam size of $\lesssim 20''$, while ours are with 61''.

L1448-IRS3: $F=2-1$ line looks similar to CS line, whereas $F=0-1$ line to N₂H⁺ line. HCO⁺ 3–2 line is significantly shifted to the red.

L1448mm: All HCN hyperfine components show the blue asymmetry like CS spectrum. On the other hand, all transitions of H₂CO and HCO⁺ have the red asymmetry.

NGC1333-2: All three lines differ from those of CS and H₂CO in their shapes. Instead, they are similar to N₂H⁺ line, which seems to be also optically thick.

L43: It shows how the absorption dip grows as the optical depth increases. The line shape of $F=2-1$ transition is quite similar to that of CS. $F=0-1$ line is relatively strong compared to the other two hyperfine lines.

L146: The shape of line profiles are closer to that of H₂CO. Lines are gradually shifted to the red, as the transition becomes optically thick. As in L43, $F=0-1$ line is brighter than $F=1-1$ line. $F=2-1$ line is quite narrow.

L483: This is a good example showing how the line shape varies with the optical depth. It seems to be consistent with a Shu (1977) type infall motion; the red shoulder in the least opaque $F=0-1$ transition changes into the absorption dip in the most opaque $F=2-1$ one. $F=2-1$ lines are more asymmetric than those of CS and H₂CO. However, the asymmetry is reversed to the red in the 20'' beam observation of HCO⁺. It is interesting to note that $F=0-1$ line is the brightest among three components. The depression of $F=2-1$ line can

not be explained by self-absorption only (see section 4).

S68N: $F=2-1$ line has a deep self-absorption with a wider blue component. The general shape of HCN resembles that of CS, though the blue wing of HCN is weaker. By contrast, H₂CO has a clear blue asymmetry.

FIRS1: This is a typical object demonstrating diverse asymmetries of different molecular transitions. $F=2-1$ component of HCN shows a prominent blue asymmetry like CS, H₂CO line does the red one, and HCO⁺ lines are nearly symmetric.

SMM4: This shows a progressive blue shift of HCN lines and deviation from symmetry with an increasing optical depth. However, the shift may not result from infall, but from outflow motion, judged from long tail to the blue. The opaque lines are similar in shape to both CS and H₂CO lines. HCO⁺ lines with the central absorption dips have the same asymmetry, but do not have any long tail to the blue.

SMM3: All three HCN components are fitted well with Gaussian. Other transitions of CS, H₂CO, and HCO⁺ are also symmetric. Relative intensities are quite close to the values of optically thin limit under the LTE condition.

B335: The asymmetry of HCN lines seems to change from the blue to the red as we move from $F=0-1$ line to $F=2-1$ one, although the S/N ratio is not so high. B335 core has been well known as a prototype of YSOs with convincing evidence of core collapse, and thus well studied (Zhou et al. 1993, 1994; Zhou 1995; Choi et al. 1995). However, our observation contradicts most existing observations (cf. Kameya et al. 1985), except CCS observations (Velusamy et al. 1995). DC 303.8-14.2 is another example showing a reversal of asymmetry among HCN hyperfine lines (Lehtinen 1997). Most observations suggestive of collapse motion have been made with a beam of $\lesssim 20''$, while observations of this study and Velusamy et al. (1995) are with $\sim 1'$ beam. Line profiles obtained with larger beams

may be contaminated by outflow motion. However, we can not rule out a possibility that the outer part of B335 is slowly expanding (Lehtinen 1997).

L1157: $F=2-1$ and $1-1$ lines have long tails to the blue with single peaks, while $F=0-1$ line is almost symmetric. Both CS and H_2CO lines show the blue asymmetry as well. On the contrary, HCO^+ lines have rather strange spectral features, the blue asymmetry in $J=3-2$ and the red one in $J=4-3$ transition.

L1251B: Shoulders in the red of $F=2-1$ and $1-1$ transitions coincide with that of CS. H_2CO has the blue asymmetry like HCN and CS, but its self-absorption is much deeper than those of HCN and CS.

In summary, for a large fraction of sources, the asymmetries are the same in all the transitions of HCN, CS, H_2CO , and HCO^+ . However, for several sources, it depends on the molecular species and, particularly for B335 and L1157, it varies from transition to transition of a molecule. It should be pointed out that the asymmetry of HCN is relatively more similar to that of CS than to that of H_2CO , which will be quantified in next subsection.

3.3. Correlations

For more detailed investigation of line profiles, one needs to quantify the line velocity associated with internal motion. We use a parameter defined by Mardones et al. (1997). At first, we measure $V_G(i-j)$, the Gaussian peak velocity in the $F=i-j$ transition of HCN after fitting the three hyperfine lines with three Gaussians. Fitting procedure is straightforward for the lines of simple shape. For lines having another weak peak or a shoulder, we fit the profile after masking such features. If intensities of two peaks differ by less than 2σ , where σ is the rms noise of spectrum, the whole velocity span is taken into account. The resulting $V_G(i-j)$ and its standard deviation of each hyperfine component are listed in Table 1. The

standard deviation is usually less than one channel width of the spectrometer. Since some hyperfine transitions of S68N, Serp FIRS1, and Serp SMM5 are blended each other, their $V_G(i-j)$ s are not included in the table. The measure of velocity shift or degree of asymmetry δV is then defined as

$$\delta V = (V_G - V_{\text{thin}})/\Delta V_{\text{thin}}. \quad (1)$$

We use the line velocity and FWHM of N_2H^+ for V_{thin} and ΔV_{thin} , respectively, in Mardones et al. (1997).

We plot relations between $\delta V(\text{HCN})$ and $\delta V(\text{CS})$, and between $\delta V(\text{HCN})$ and $\delta V(\text{H}_2\text{CO})$ in Fig. 2. The velocity shifts of CS and H_2CO molecules are also from Mardones et al. (1997). It is found that $\delta V(0-1)$ correlates well with $\delta V(\text{CS})$. And we do not find any significant differences in their relations between class 0 and I. The close relation itself implies that HCN $F=0-1$ transition probes as similar kinematics as CS molecule does. It would be possible only if the distribution of HCN molecule is similar to that of CS inside the core. However, the slope of 0.47 suggests that $F=0-1$ transition is moderately optically thick; if the transition is as thin as that of N_2H^+ , the slope should be around zero. It would not be so optically thick, since their line shapes are usually simple and show a single peak. The slope significantly less than unity may also be due to a difference in the beam size of two surveys; our larger telescope beam, which covers more volume of static envelope, may lessen the slope.

As going toward the $F=2-1$ transition, we notice the worse correlation as well as the gradual increase of the slope. The increase of the slope up to around unity implies that the most opaque line of HCN is as sensitive to the internal motion of the core as the CS, again suggesting similar spatial distributions of both HCN and CS molecules. General similarity in the line shapes between HCN $F=2-1$ and CS $J=2-1$, as shown in the previous subsection, supports this argument. An increasing scatter can be interpreted in terms of the

opacity of the transition; since the opaque line is formed where the optical depth is about one, it does not reflect a global property, but does a local one. Thus small differences in excitation conditions and chemistry between HCN and CS would result in large differences in their line profiles.

In the lower panel of Fig. 2, we plot the relations between $\delta V(\text{HCN})$ and $\delta V(\text{H}_2\text{CO})$. The correlation between them is not so good as the case of $\delta V(\text{HCN})$ and $\delta V(\text{CS})$; we can hardly find a linear relationship between $\delta V(0-1)$ and $\delta V(\text{H}_2\text{CO})$. Their distributions mimic the relation between $\delta V(\text{CS})$ and $\delta V(\text{H}_2\text{CO})$ illustrated in Fig 3, which is drawn from data set of Mardones et al. (1997). However, if we confine ourselves to the sources of $\delta V(\text{HCN}) < 0$ and $\delta V(\text{H}_2\text{CO}) < 0$, then we can see as similar trend as in the upper panel – the concomitant increase of the slope to unity with the optical depth.

Good correlations of δV s between HCN and CS indicate a similar distribution of both molecular species in the core. It is intriguing that, in spite of the larger beam size of our HCN observation, the slope is roughly unity for both pairs of $\delta V(\text{HCN})$ – $\delta V(\text{CS})$ and $\delta V(\text{HCN})$ – $\delta V(\text{H}_2\text{CO})$ for the most opaque transition of HCN. It appears that HCN is even more sensitive to the internal motion of the core. The critical density of HCN $J=1-0$, $2.5 \times 10^6 \text{ cm}^{-3}$, is larger than those of CS and H_2CO , $5.7 \times 10^5 \text{ cm}^{-3}$ and $1.1 \times 10^6 \text{ cm}^{-3}$, respectively. Thus HCN molecule traces deeper and denser regions of YSOs than CS or H_2CO . If HCN lines are observed with as similar beam size as that of CS or H_2CO ($\sim 20''$), we may be able to see more clearly the internal motion of the cores.

Fig. 4 quantifies the $\delta V(\text{HCN})$ of individual sources as a function of relative optical depth. If there is any systematic internal motion, we may expect gradual increase or decrease of δV (Myers et al. 1995; Zhang et al. 1998). It was not so easy to find such a relation from combinations of different molecules or transitions often sparsely distributed in frequency space, since the chemistry and beam size are different from each other. Most

YSOs exhibit a monotonic increase or decrease of δV with respect to the optical depth. Seven sources (L1448mm, NGC1333-4A, L483, Serp SMM4, L1157, L1172, and L1251B) suggest infall motion, while three sources (L43, L146, and B335) do outward motion. A few YSOs (L1448-IRS3, serp SMM3, and 18331-0035) seem to be static. A few large blobs or clumps may also give rise to such a systematic velocity shift. This possibility is, however, ruled out by the smoothness of optically thin N_2H^+ lines which are almost symmetric.

4. Radiative Transfer Model of L483

Line profiles of L483 in Fig. 1 demonstrate clearly how the absorption dip develops under inward velocity field as the optical depth increases. Line intensity ratios among hyperfine transitions significantly deviate from the ‘standard hyperfine ratios’ (see section 5). Thus, synthesizing them with radiative transfer code will be useful in understanding the infall motion as well as structure of L483. We do not try to reproduce detailed features of the observed line profiles, but focus on quantitative comparisons between observed and synthesized lines.

The radiative transfer of HCN is complicated due to line overlap caused by hyperfine splitting of energy levels. In the case of cold cores like L483, the hyperfine lines do not overlap each other in $J=1-0$ transition, but they do in the transitions of higher J s, which affects the excitation condition of $J=1-0$ transition. The problem of the line overlap has been successfully treated by the Monte Carlo method (González-Alfonso & Cernicharo 1993; Lapinov 1989) as well as by a conventional one (Turner et al. 1997). We will use the former scheme and impose the condition of infall motion. Levels up to $J=4$ are taken into account, which include 13 individual energy levels and 21 radiative transitions among them. The Einstein A coefficients and line frequencies are provided by González-Alfonso (1998) and by Turner (1998), and the collisional rate coefficients by Monteiro & Stutzki (1986).

With those molecular constants, we made a model of one dimensional radiative transfer, and confirmed its performance, by reproducing results of González-Alfonso & Cernicharo (1993).

The Shu model (Shu 1977) could be a start point for the distributions of gas density and motion inside the core. Based on the observation of high density tracing molecules, HC_3N and NH_3 (Fuller & Myers 1993), we fix the size of the core as 1.72 or $R = 0.10$ pc at a distance of 200 pc. The core is divided into 30 concentric shells with radii running as $r_i \propto i^{0.7}$ ($i = 0, \dots, 30$). Since temperature is found to be 12 K near the *IRAS* source and fall to 9 K in the outer region (Fuller & Myers 1993; Parker et al. 1991), T_k is assumed to be constant at 10 K in the first set of calculations. The sound speed is then 0.2 km s⁻¹. An e-folding non-thermal turbulence of $v_{\text{turb}} = 0.4$ km s⁻¹ is found from Myers et al. (1995), and the abundance of HCN relative to H_2 , 5×10^{-9} is from Turner et al. (1997) and from González-Alfonso & Cernicharo (1993). Model calculations are then carried out and resulting line profiles are convolved with the telescope beam. In order to compare the synthetic line profile with the observed one in brightness temperature unit, we divided the latter one by 0.5, a compromise between the main beam efficiency (0.4) and the forward beam coupling efficiency (0.7).

The Shu model is completely described by an infall radius, r_{inf} or an elapsed time after the onset of infall. Fig. 5 shows synthesized line profiles for $r_{\text{inf}} = 0, 0.4R$, and $0.8R$, respectively. From the synthesized lines (top in Fig. 5), we find that i) the asymmetry is negligible in three hyperfine lines, ii) the synthesized lines are weaker than the observed ones, and iii) the line intensity ratios are maintained as $I(F = 0 - 1) : I(F = 1 - 1) : I(F = 2 - 1) = 1 : (1.3 - 2) : (2 - 3)$. Then we applied the kinetic temperature varying as $T_k(r) = 10(R/r)^{0.4}$ K, where the $r^{-0.4}$ dependence is based on the distribution of dust temperature (Myers et al. 1995; Wang et al. 1995). The

sound speed was accordingly changed to 0.25 km s^{-1} . In fact, the Shu model assumes ‘isothermal’ cloud, and thus the model with kinetic temperature decreasing outward is far from consistency. However, we need to assume ‘constant’ sound speed in order to use his simple expression of density and velocity field. With this new temperature distribution, the synthetic lines (middle in Fig. 5) become stronger and more asymmetric. However, the $F=0-1$ line is still weaker than the observed one, and the hyperfine ratios differ from observation. It appears that the inside-out collapse model can not produce the observational features well. One viable option is to increase the density of Shu model core and to introduce an extended diffuse envelope, as proposed by Wang et al. (1995) and by González-Alfonso & Cernicharo (1993). The role of the diffuse envelope is to attenuate the optically thicker line more. A large turbulence in the envelope is required for rather uniform attenuation across the line. If the envelope is sufficiently opaque, the line core of $F=2-1$ component may be formed in the envelope. The general weakening of lines is then compensated by an augmentation of density in the core. A successful fit after several trial and errors is shown in the bottom of Fig. 5. The resulting model is that a core with $r_{\text{inf}} = R = 0.1 \text{ pc}$ and $v_{\text{turb}} = 0.3 \text{ km s}^{-1}$ is embedded in a static envelope with $R = 0.3 \text{ pc}$, $n(\text{H}_2) = 5 \times 10^3 \text{ cm}^{-3}$, $v_{\text{turb}} = 1 \text{ km s}^{-1}$, and $T_k = 10 \text{ K}$. In the core, the density increases by a factor of 6 and the infall velocity decreases by a factor of 2 with respect to those of the Shu model, respectively. The line center optical depths of $F=0-1$, $1-1$, and $2-1$ transitions towards the center of core are 3, 8, and 11, respectively, which are not beam averaged. The difference in peak brightness temperature is, of course, due to different excitation temperatures of the transitions. The red shift of absorption dip shown in Fig. 1b justifies rather large infall radius; without the inward motion of outer layer, the absorption dip will be located at the velocity of optically thin line. The size and density of envelope may change in such a way that its optical depth is kept constant. Different combinations, however, give rise to deeper or shallower absorption dips due to different excitation conditions of HCN in the envelope.

Thus, we come to a model different from that of Shu (1977), as invoked already by Wang et al. (1995). In fact, higher density and slower infall speed are characteristic features of a magnetically supported core model, where the contraction occurs quasi-statically and the density of envelope increases as the core evolves (Ciolek & Mouschovias 1994, 1995).

Obviously, the real structure of L483 seems to be more complex than our model. It is shown that a near IR image exhibits an elongated structure in the East-West direction and the axis of CO molecular outflow is also aligned in this direction (Parker et al. 1991; Ladd et al. 1991; Fuller et al. 1995). Gregersen et al. (1997) noticed that $\text{HCO}^+ J=3-2$ and $4-3$ lines show the red asymmetry, contrary to ours. However, the possibility of outward motion suggested by HCO^+ near the center is ruled out by the recent VLA observation of NH_3 indicating inward motion down to $\sim 0''.2$ scale (Fuller & Wootten 1999). Reasons for different asymmetry of HCO^+ may be attributable to differences in molecular chemistry and excitation conditions (see section 5).

5. Discussions

The similarity of line shapes between CS and HCN and the dissimilarity between HCO^+ and HCN were already mentioned in section 3. We further examine the line asymmetries of 9 class 0 objects which have been observed in all transitions of four molecular species (CS, H_2CO , HCN, and HCO^+). As summarized in Table 2, only one source each shows the reversal of asymmetry between CS and HCN, and between HCO^+ and H_2CO . On the other hand, three sources change their asymmetries between HCN and HCO^+ . Thus, though the number of samples is not large, it seems that the line asymmetry is similar within each pair of CS–HCN and $\text{HCO}^+–\text{H}_2\text{CO}$, but different between two pairs. It is interesting to note that CS and probably HCN seem to prefer the blue asymmetry compared with HCO^+ .

Why do the two pairs show different asymmetry? Let us first consider if the critical densities of four molecules are grouped in the same way as their line shapes. A sequence of transitions is, however, CS 2–1, H₂CO 2₁₂–1₁₁, HCN 1–0, and HCO⁺ 3–2 & 4–3 in an order of increasing critical density (The critical densities of HCO⁺ 3–2 and 4–3 are 0.5×10^7 and 1.3×10^7 cm^{–3}, respectively; Monteiro 1985), suggesting that excitation condition is of little importance. Then molecular chemistry such as depletion in the innermost region and enhancement in the outflow may play important roles in the line formation. It is known that HCN as well as CS may freeze out onto grains in cold dense region (Bergin et al. 1995; Blake et al. 1992; McMullin et al. 1994), whereas HCO⁺ will not, since it has a small dipole moment and there is no chemical reaction route to consume it in this region (Rawlings 1996; van Dishoeck, E.F. & Blake, G.A. 1998). However, there seems to be little observational evidence of significantly depleted CS or HCN. If so, the blue asymmetry would be more frequent in HCO⁺ than in CS or HCN, provided that motion is more like inside-out collapse, which is usually confined to the central region of core. However, this is not the case, as shown in Table 2.

Outflows prevalent in these sources may make certain molecules more abundant. L1157 is one of the examples which shows dramatic enhancements of various kinds of molecules (Bachiller & Pérez Gutiérrez 1997), where four molecules of our concern, CS, H₂CO, HCN, and HCO⁺ are all enhanced. In the interferometric observations of 9 class 0 objects, HCO⁺ and HCN show so different sensitivity to the envelope and outflow from source to source that one could not find any general tendency (Choi et al. 1999). Recent BIMA observation of L483 suggests that HCO⁺ traces outflow, while HCN does thick disk or envelope (Park et al. 1999). The molecular chemistry is very complicated in this way, if both outflow and infalling envelope coexist; even in the case that the outflow occupies a small fraction of volume, the line shape will be significantly affected, if the abundance increases drastically (e.g., > 100) in the flow region. The chemistry may also be related with the evolution

of YSOs. Observations with high spatial resolution and more elaborated time-dependent chemistry models are required for further understanding of line formation and molecular chemistry in YSOs (Mundy et al. 1995).

We noted in section 3 that hyperfine line intensities of Serp SMM4 and SMM3 are scaled to the relative LTE optical depth. It is also interesting to note that, despite of their strong self-absorptions, the intensity ratios of three sources, S68N, Serp FIRS1, and SMM5, are also close to $1 : 3 : 5$, an optically thin limit in the LTE condition. In Fig. 6, excluding these three sources, we plot the hyperfine line ratios, R_{02} and R_{12} , defined by,

$$R_{02} = \frac{T_{\max}(F = 0 - 1)}{T_{\max}(F = 2 - 1)}, \quad R_{12} = \frac{T_{\max}(F = 1 - 1)}{T_{\max}(F = 2 - 1)}. \quad (2)$$

It is found that R_{12} lies between 0.4 and 0.7, except one source, while R_{02} spans from 0.2 to 1.0. Similar distributions have been known for quiescent dark clouds (Harju 1989; González-Alfonso & Cernicharo 1993) and for small translucent cores (Turner et al. 1997), though their physical conditions are quite different each other. The parameter space with $R_{12} \lesssim 1$ and $R_{02} \lesssim 0.8$ can be explained in terms of radiative transfer effect on the clouds/cores which are either static or under systematic motion (González-Alfonso & Cernicharo 1993; Turner et al. 1997). However, the region of $R_{12} \gtrsim 1$ or $R_{02} \gtrsim 0.8$, where the $F=2-1$ component is significantly suppressed with respect to the $F=0-1$ and $F=1-1$ components, seems to invoke the existence of diffuse envelope, as we have shown in section 4.

Recently, Afonso et al. (1998) carried out an HCN $J=1-0$ survey towards YSOs in Bok globules. They found that HCN is detected with a higher probability in class I and probably class 0 objects than in starless cores and class II sources. Because there is only one class 0 source in their survey, such a preference for class 0 was uncertain. Our study implies the high detection rate of almost unity for both class 0 and I sources. Thus there seems to be a unique phase of class 0 and I in the evolution of YSOs when a dense envelope

of $\sim 1'$ ($0.05 - 0.1$ pc at the distances of $150 - 300$ pc) in size is formed.

6. Summary

We have carried out a survey of HCN $J=1-0$ hyperfine lines for 24 objects identified as class 0 and I with a spectral resolution of 0.068 km s^{-1} . 22 sources are detected with around 30 mK rms level in T_A^* unit.

It is found that three hyperfine components show a variety of spectral features such as deep self-absorption, asymmetry, and broad wings which are more prominent in the optically thicker lines. Moreover, for a large fraction of sources, HCN hyperfine lines show a progressive shift to the blue, as the optical depth increases. Only a few sources show a gradual shift to the red, which implies that an inward motion is predominant in the core embedding YSOs. When compared with previous CS and H₂CO surveys, the velocity shifts of HCN correlate better with those of CS than with those of H₂CO. Little difference in the correlation is noted between class 0 and I.

L483 is confirmed as a candidate infalling source on ~ 0.1 pc scale, from a growing degree of asymmetry and self-absorption with an increasing optical depth. We synthesized its hyperfine lines, by solving radiative transfer in a collapsing core model with the Monte Carlo method. The synthetic lines based on the Shu (1977) model do not fit the observed ones. We reproduced the observed ones successfully with the modification of the Shu model, an overall increase of gas density by a factor of 6 and the decrease of infall velocity by a factor of 2. Furthermore, in order to explain the line intensity ratios, a diffuse, static, and geometrically thick envelope surrounding the modified Shu core is essential.

Authors are grateful to Dr. C.W. Lee and Dr. E. González-Alfonso for helpful discussions. This study was supported by Korea Astronomy Observatory through KAO

grant 97-5400-000.

REFERENCES

Afonso, J. M., Yun, J. L., Clemens, D. P., 1998, AJ, 115, 1111

Bachiller, R., Pérez Gutiérrez, M., 1997, ApJ, 487, L93

Bergin, E. A., Langer, W. D., Goldsmith, P. F., 1995, ApJ, 441, 222

Blake, G. A., van Dishoeck, E. F., Sargent, A., 1992, ApJ, 391, L99

Choi, M., Evans, N. J. II., Gregersen, E. M., Wang, Y., ApJ, 448, 742, 1995

Choi, M., Panis, J.-F., Evans, N. J. II., 1999, ApJ, accepted

Ciolek, G. E., Mouschovias, T. Ch., 1994, ApJ, 425, 142

Ciolek, G. E., Mouschovias, T. Ch., 1995, ApJ, 454, 194

Fuller, G. A., Lada, E. A., Masson, C. R., Myers, P. C., 1995, ApJ, 453, 754

Fuller, G. A., Myers, P. C., 1993, ApJ, 418, 273

Fuller, G. A., Wooten, A., 1999, ApJ, submitted

González-Alfonso, E. 1998, private communication

González-Alfonso, E., Cernicharo, J. 1993, A&A, 279, 506

Green, S., Chapman, S., 1978, ApJS, 37, 169

Green, S., Garrison, B. J., Lester, Jr., W. A., Miller, W. H., 1978, ApJS, 37, 121

Gregersen, E. M., Evans, N. J. II., Zhou, S., Choi, M., 1997, ApJ, 484, 256

Harju, J., 1989, A&A, 219, 293

Kameya, O., Hasegawa, O., Hirano, N., Takakubo, K., Seki, M., 1985, in IAU Symp. 115, Star Forming Regions, ed. M. Peimbert and J. Jugaku (Dordrecht: Reidel), 366

Ladd, E. F., Adams, F. C., Casey, S., Davidson, J. A., Fuller, G. A., Harper, D. A., Myers, P. C., Padman, R., 1991, *ApJ*, 366, 203

Lapinov, A. V., 1989, *Sov. Astron.*, 33, 132

Lehtinen, K., 1997, *A&A*, 317, L5

Lovas, F. J., 1992, *J. Phys. Chem. Ref. Data*, 21, 181

Mardones, D., Myers, P. C., Tafalla, M., Wilner, D. J., Bachiller, R., Garay, G., 1997, *ApJ*, 489, 719

McMullin, J. P., Mundy, L. G., Blake, G. A., 1994, *ApJ*, 437, 305

Monteiro, T. S., 1985, *MNRAS*, 214, 419

Monteiro, T. S., Stutzki, J., 1986, *MNRAS*, 221, 33p

Mundy, L. G., McMullin, J. P., Blake, G. A., 1995, *ApSS*, 224, 81

Myers, P. C., Bachiller, R., Caselli, P., Fuller, G. A., Mardones, D., Tafalla, M., Wilner, D. J., 1995, *ApJ*, 449, L65

Narayanan, G., Walker, C. K., Burkley, H. D., 1998, *ApJ*, 496, 292

Park, Y.-S. et al., 1999, in preparation

Parker, N. D., Padman, R., Scott, P. F., 1991, *MNRAS*, 252, 442

Rawlings, J. M. C., 1996, *ApSS*, 237, 299

Shu, F. H., 1977, *ApJ*, 214, 488

Turner, B. E., 1998, private communication

Turner, B. E., Pirogov, L., Minh, Y. C., 1997, *ApJ*, 483, 235

van Dishoeck, F.F., Blake, G.A., 1998, *ARA&A*, 36, 317

Velusamy, T., Kuiper, T. B. H., Langer, W. D., 1995, *ApJ*, 451, L75

Wang, Y., Evans, N. J. II., Zhou, S., Clemens, D. P., 1995, *ApJ*, 454, 217

Zhang, Q., Ho, P. T. P., Ohashi, N., 1998, *ApJ*, 494, 636

Zhou, S., 1995, *ApJ*, 442, 685

Zhou, S., Evans, N. J. II., Kömpe, C., Walmsley, C. M., 1993, *ApJ*, 404, 232

———, 1994, *ApJ*, 421, 854

Fig. 1.— *a-d*. The observed line profiles of HCN. Three hyperfine components of $F=0-1$ (bottom), $F=1-1$ (middle), and $F=2-1$ (top) are aligned in order to see any systematic changes in their line shapes and positions with optical depth. In each panel, a vertical line marks the LSR velocity determined by the optically thin N_2H^+ 1–0 transition (Mardones et al. 1997). For Serp SMM2, HC^{18}O^+ 3–2 line is used instead (Gregersen et al. 1997).

Fig. 2.— The relation between $\delta V(\text{HCN})$ and $\delta V(\text{CS})$ and between $\delta V(\text{HCN})$ and $\delta V(\text{H}_2\text{CO})$, where filled circles are for class 0, and filled squares for class I. We derive linear relations (solid lines) of the form $y = ax$ by least square fit, assuming noise in *both* variables. In the top right are linear correlation coefficients. Error bars of $\pm 1\sigma$ in the lower right corners are the largest ones among these sources.

Fig. 3.— The relation between $\delta V(\text{CS})$ and $\delta V(\text{H}_2\text{CO})$. Data are from Mardones et al. (1997). Circles and squares represent class 0 and I, respectively. Same as in Fig. 2 for the error bars.

Fig. 4.— The $\delta V(\text{HCN})$ as a function of the relative optical depth. The optical depth of N_2H^+ is assumed to be zero. Error bars of $\pm 1\sigma$ are indicated for each source. Vertical offsets are arbitrary.

Fig. 5.— The comparison of synthetic (lines) and observed (histogram) line profiles of L483. Top three profiles are from the standard Shu model with a constant T_k of 10 K. Solid, dotted, and dashed lines correspond to $r_{\text{inf}} = 0, 0.4R$, and $0.8R$, respectively. Three profiles in the middle are from the standard Shu model with a temperature variation of $T_k = 10(r/R)^{-0.4}$ K. Notations are the same as above. Two in the bottom are the profiles of the best fit and the observed ones. See text for model parameters of the best fit.

Fig. 6.— The distribution of intensity ratios of HCN hyperfine lines, R_{12} and R_{02} (see text for definition). A solid line represents a locus under the LTE condition; the R_{12} and R_{02} approach to unity, as the transition becomes opaque.

Table 1. List of sources and their line velocities

Name	RA(1950) <i>h m s</i>	DEC(1950) $^{\circ} \ ' \ '$	class ^a	V_G (km s $^{-1}$)		
				$F=0-1$	$F=1-1$	$F=2-1$
L1448-IRS3	3 22 31.5	30 34 49	0	4.53 \pm 0.02	4.52 \pm 0.02	4.54 \pm 0.01
L1448mm	3 22 34.4	30 33 35	0	4.76 \pm 0.03	4.84 \pm 0.02	4.82 \pm 0.02
NGC1333-2	3 25 49.9	31 04 16	0	7.65 \pm 0.04	7.59 \pm 0.03	7.50 \pm 0.02
NGC1333-4A	3 26 04.8	31 03 13	0	7.04 \pm 0.04	6.76 \pm 0.02	6.70 \pm 0.01
L43	16 31 37.7	-15 40 52	I	0.58 \pm 0.01	0.54 \pm 0.02	0.71 \pm 0.01
L146	16 54 27.2	-16 04 48	I	5.25 \pm 0.01	5.24 \pm 0.02	5.34 \pm 0.01
L483	18 14 50.6	-04 40 49	0	5.30 \pm 0.01	5.11 \pm 0.03	5.05 \pm 0.02
S68N	18 27 15.2	01 14 57	0
Serp FIRS1	18 27 17.4	01 13 16	0
Serp SMM5	18 27 18.9	01 14 36	0
Serp SMM4	18 27 24.3	01 11 11	0	7.81 \pm 0.03	7.62 \pm 0.02	7.71 \pm 0.01
Serp SMM3	18 27 27.3	01 11 55	0	7.80 \pm 0.03	7.70 \pm 0.01	7.68 \pm 0.01
Serp SMM2	18 27 28.0	01 10 45	0	7.45 \pm 0.03	7.30 \pm 0.02	7.28 \pm 0.01
18331-0035	18 33 07.6	-00 35 48	0	10.86 \pm 0.03	10.81 \pm 0.02	10.89 \pm 0.01
L723	19 15 41.3	19 06 47	0
L673A	19 18 04.6	11 14 12	0	7.02 \pm 0.02	6.94 \pm 0.01	6.99 \pm 0.01
B335	19 34 35.7	07 27 20	0	8.38 \pm 0.02	8.39 \pm 0.02	8.60 \pm 0.01
IRAS20050	20 05 02.5	27 20 09	0
L1152	20 35 19.4	67 42 30	I	2.67 \pm 0.01	2.65 \pm 0.02	2.62 \pm 0.01
L1157	20 38 39.6	67 51 33	0	2.60 \pm 0.02	2.38 \pm 0.02	2.31 \pm 0.01
L1172	21 01 44.2	67 42 24	I	2.84 \pm 0.02	2.60 \pm 0.02	2.57 \pm 0.02
L1251A	22 34 22.0	75 01 32	I	-4.90 \pm 0.04	-4.98 \pm 0.04	-5.15 \pm 0.02
L1251B	22 37 40.8	74 55 50	I	-3.94 \pm 0.03	-4.06 \pm 0.03	-4.13 \pm 0.01
L1262	23 23 48.7	74 01 08	I	4.12 \pm 0.02	4.08 \pm 0.03	4.25 \pm 0.02

^a Sources are classified as class 0, if $T_{bol} \leq 80$ K, and class I, otherwise.

Table 2. Line asymmetry

Name	CS 2–1	$\text{H}_2\text{CO } 2_{12}-1_{11}$	$\text{HCO}^+ 4-3$	$\text{HCO}^+ 3-2$	$\text{HCN } F=2-1$
L1448-IRS3	R	R	...	R	N
L1448mm	B	R	R	R	B
NGC1333-4A	B	B	B	B	B
L483	B	B	R	R	B
Serp FIRS1	B	R	N	N	B
Serp SMM4	B	B	B	B	B
Serp SMM3	R	N	N	N	N
B335	B	B	B	B	R
L1157	B	B	R	B	B

R and B indicate the red and blue asymmetries, respectively, while N means near symmetry. Asymmetries of CS 2–1 and $\text{H}_2\text{CO } 2_{12}-1_{11}$ are from Mardones et al. (1997), and those of $\text{HCO}^+ 4-3$ and 3–2 from Gregersen et al. (1997).

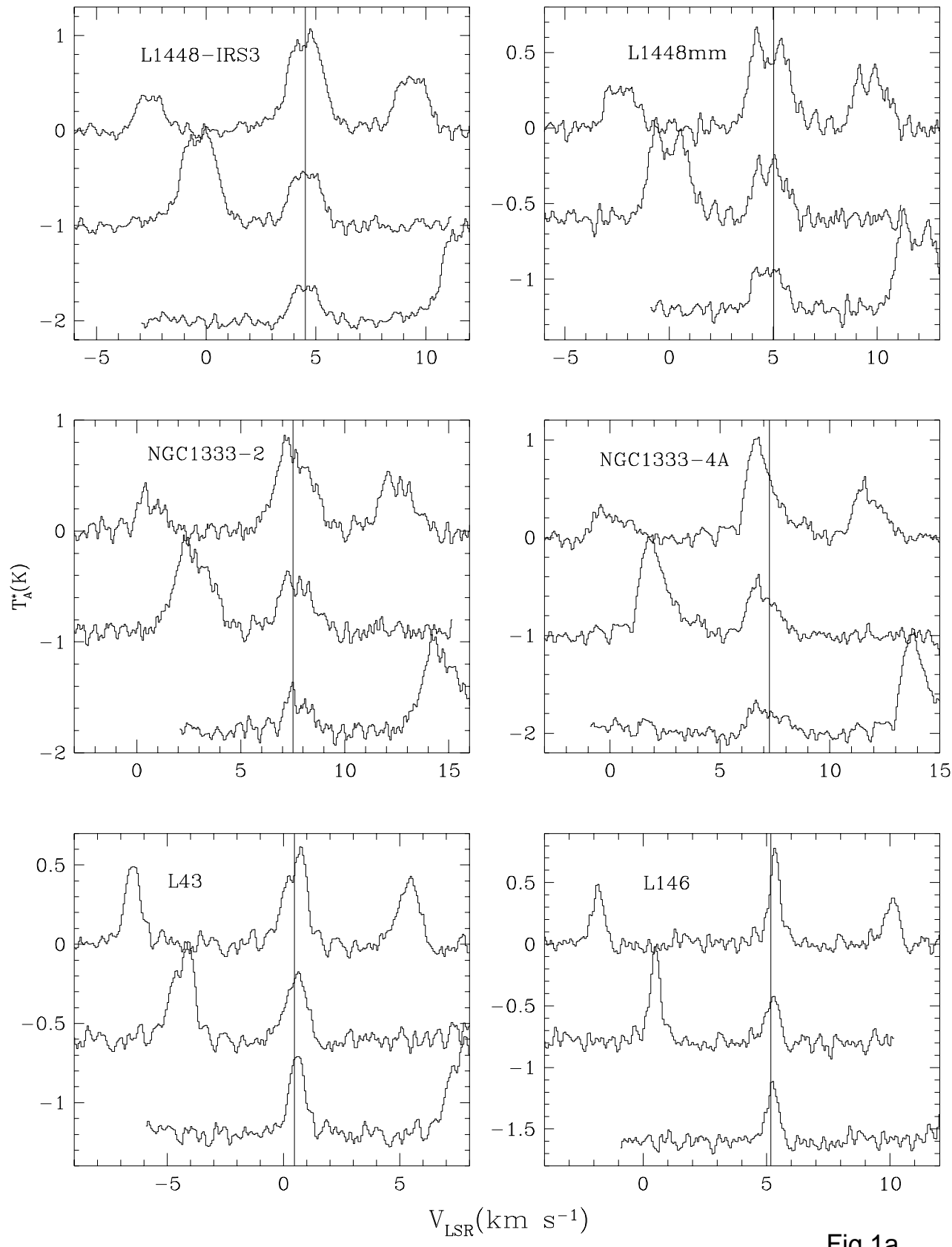


Fig.1a

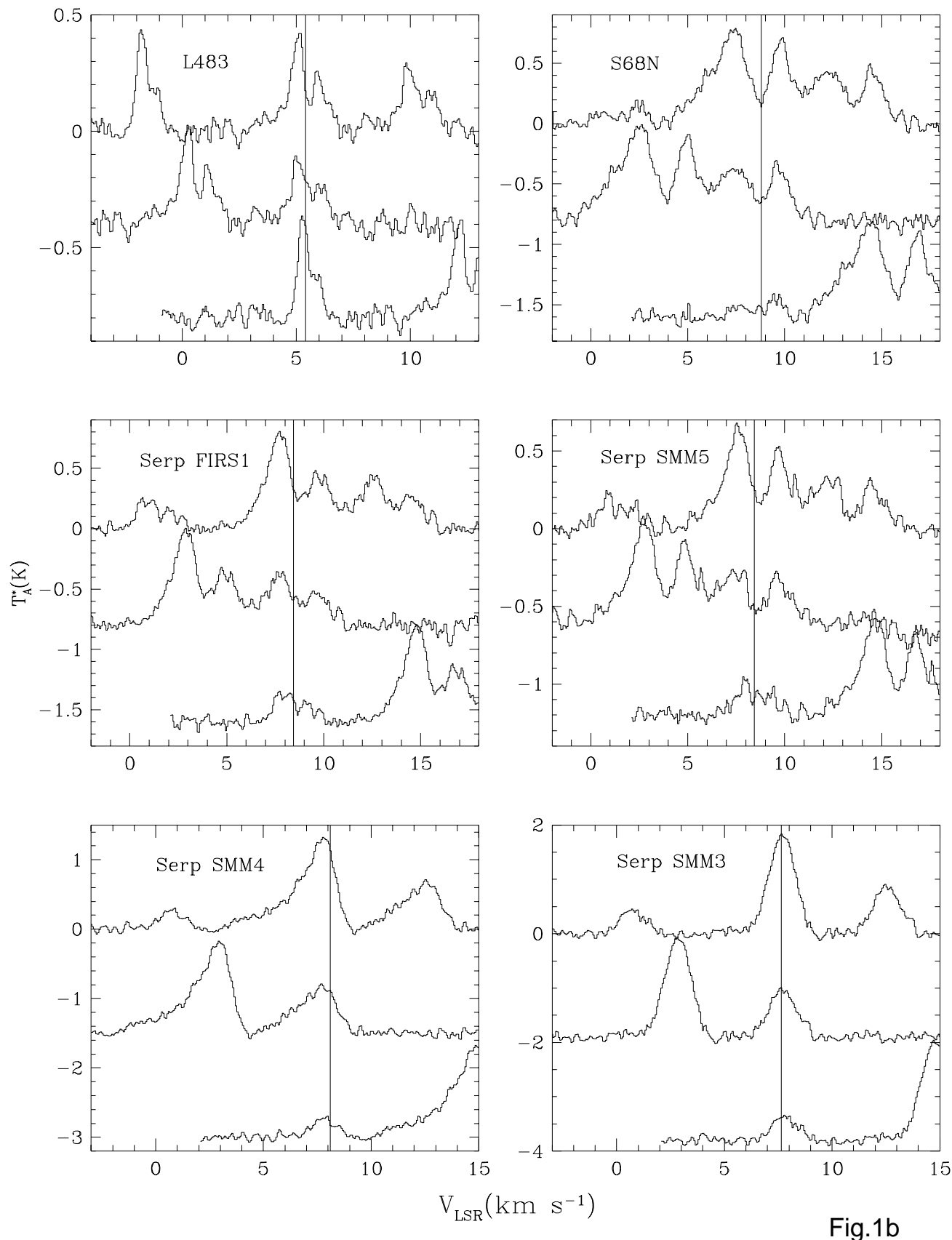


Fig.1b

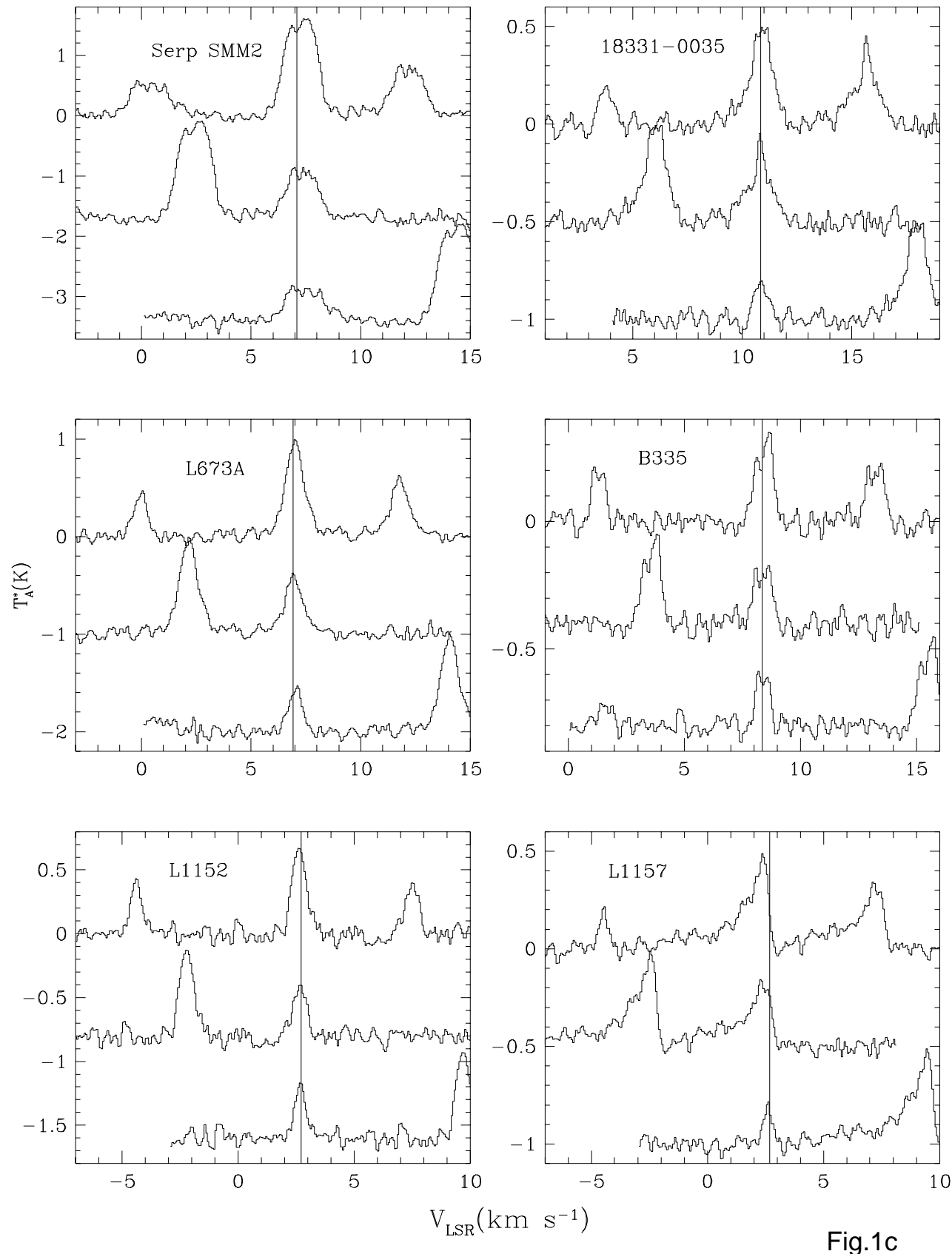


Fig.1c

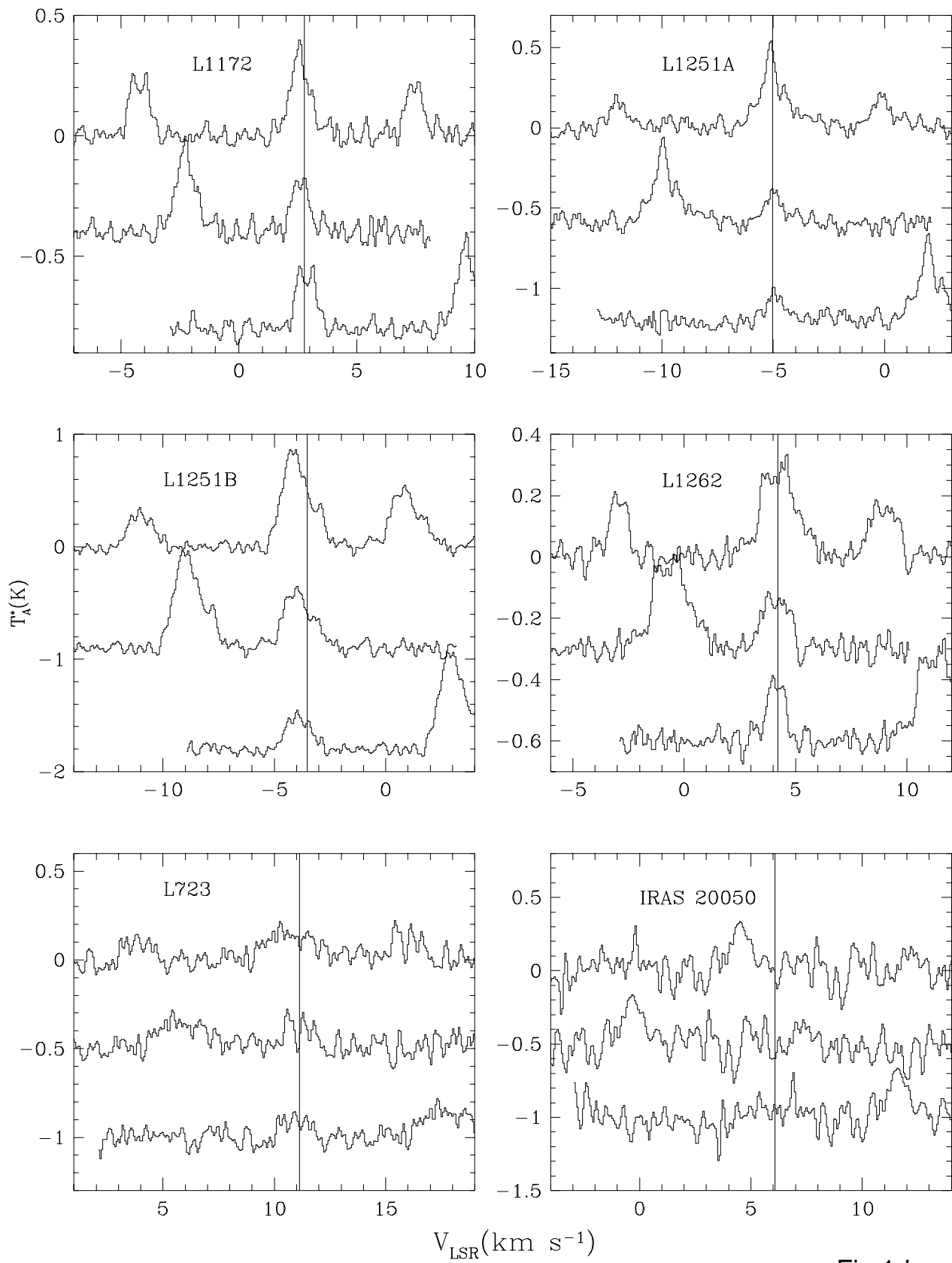


Fig.1d

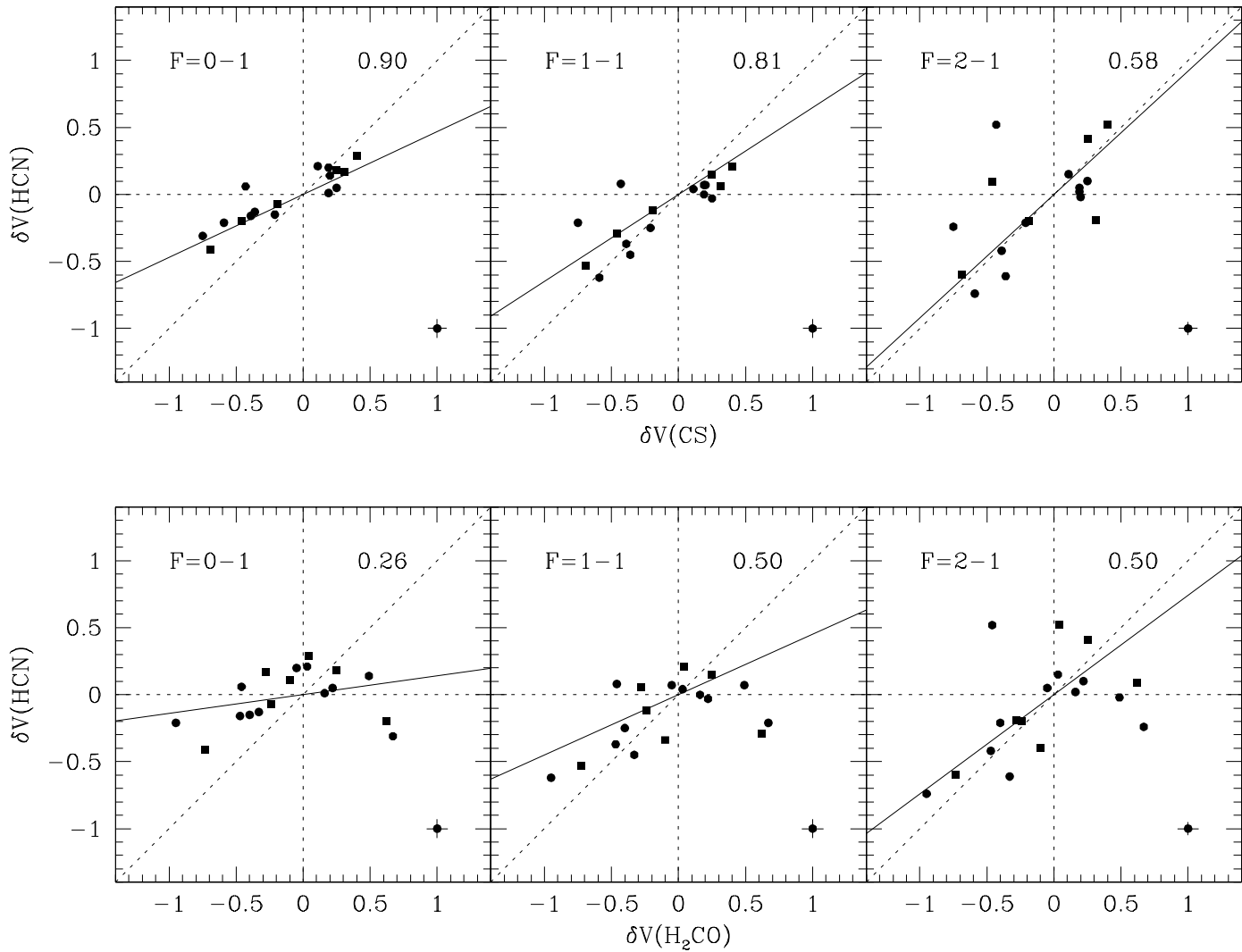


Fig.2

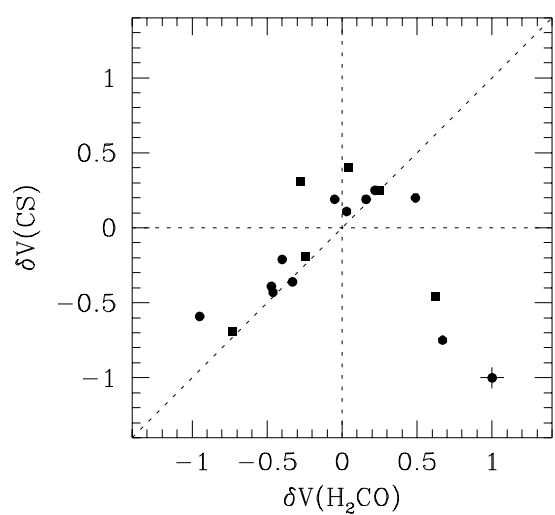


Fig.3

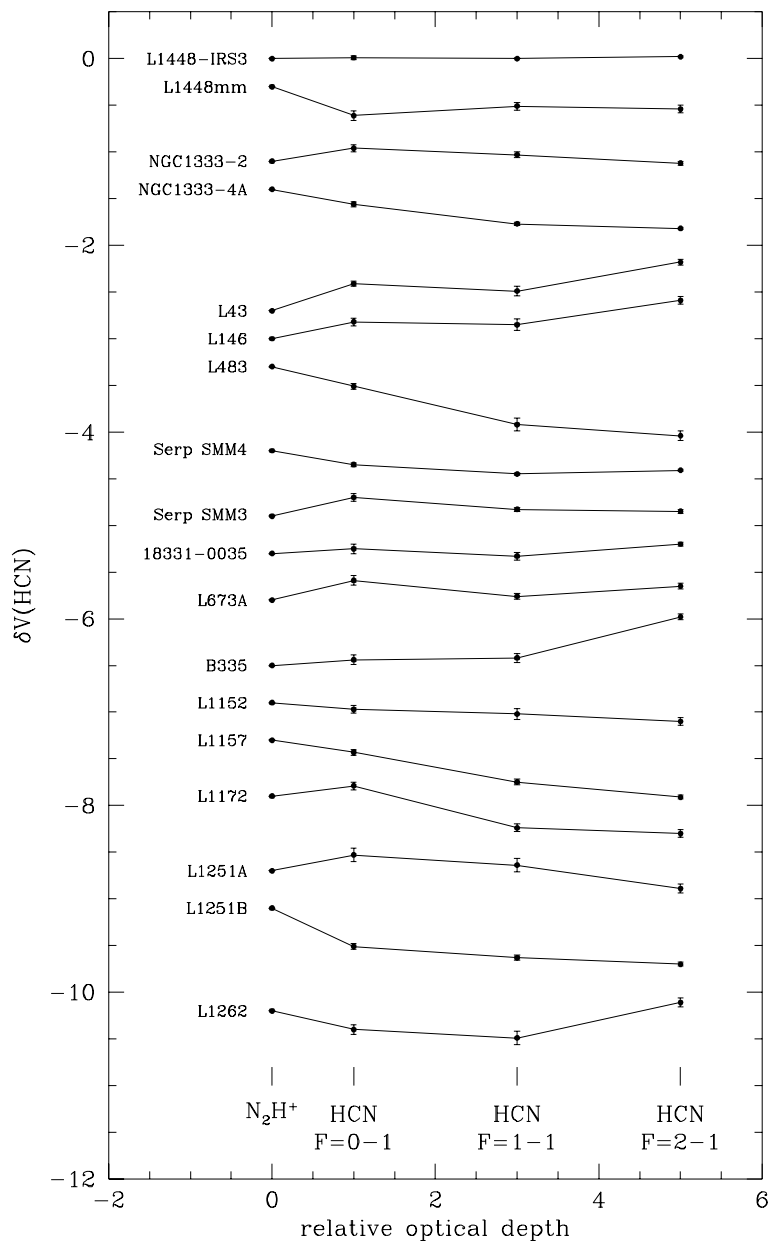


Fig.4

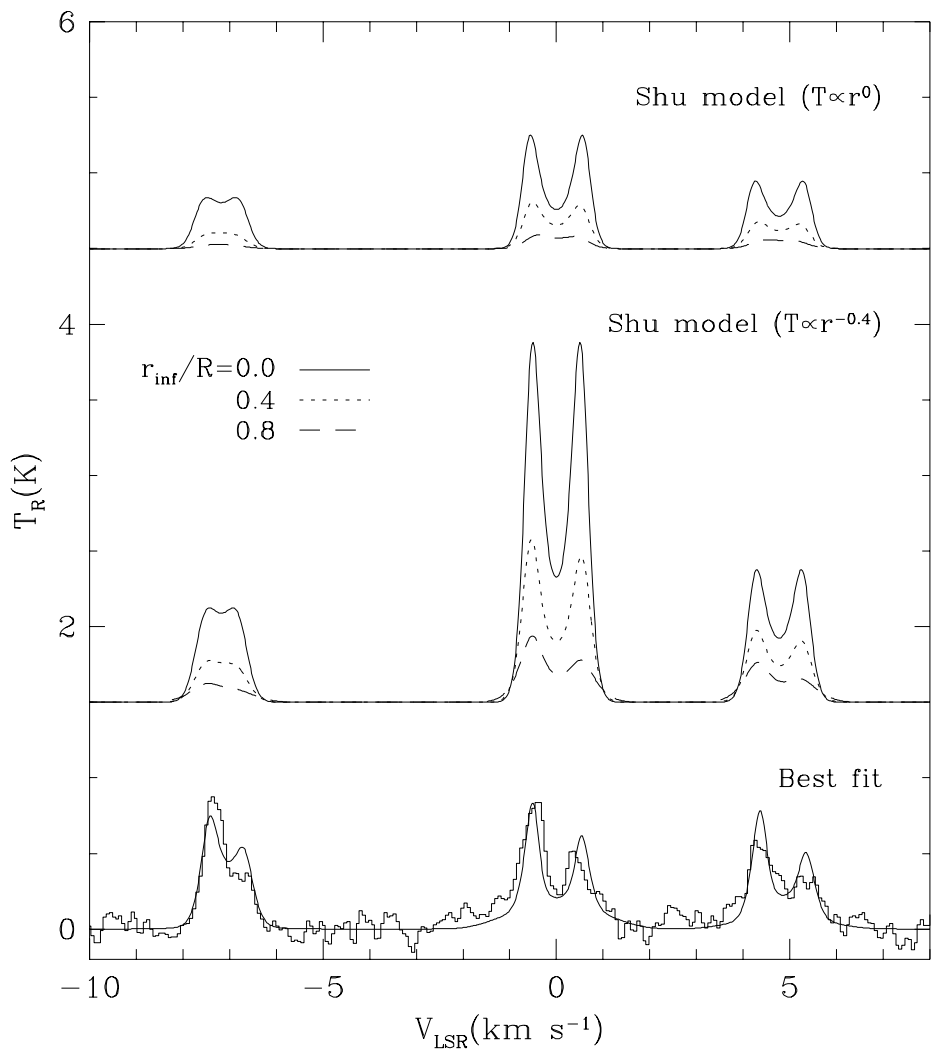


Fig.5

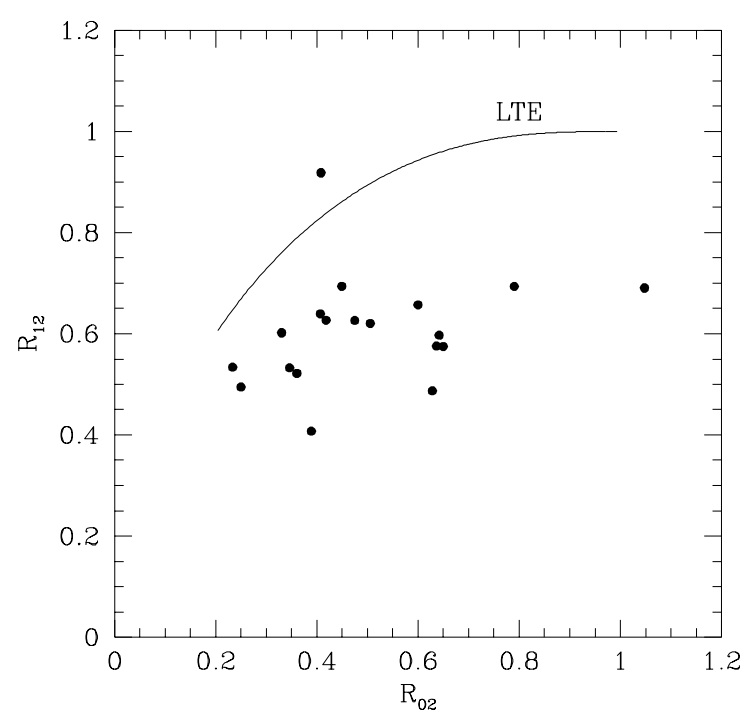


Fig.6